Numerical simulation of film instability over a corrugated sheet

Journal of Physics: Conference Series **2940** (2025) 012010 doi:10.1088/1742-6596/2940/1/012010

Numerical simulation of film instability over a corrugated sheet

Nicola Suzzi and Giulio Croce

DPIA - Dipartimento Politecnico di Ingegneria e Architettura - Universitá di Udine - Via delle Scienze - 33100 - Udine (UD) - Italy

E-mail: nicola.suzzi@uniud.it, giulio.croce@uniud.it

Abstract. The evolution of a liquid layer flowing down a corrugated sheet driven by gravity, which is the characteristic configuration of structured packing, is numerically analysed via the solution of the governing lubrication equation, which reduces the 3D physical problem to a 2D mathematical problem. Disjoining pressure is used to model contact line dynamics and surface wettability, while full implementation of capillary pressure allows to investigate contact angles up to 60°. The effect of corrugation is introduced via the definition, in the governing lubrication equation, of non-uniform gravity acceleration. Furthermore, the additional capillary force, arising from variations in the solid surface curvature, is also implemented. Different corrugation geometries and flow conditions, the latter being defined by the reference film Capillary number, are investigated, looking for configurations that allow enhancement of the liquid-gas interface area at low liquid flow rate. Such an analysis provides a novel approach in the design of structured packing, widely used in carbon capture via chemical absorption.

1 Introduction

The evolution of a thin liquid layer is involved in a number of practical applications, such as the in-flight icing [1, 2] and the CO2 absorption through structured packing [3, 4, 5]. In the absorption process through structured packing, the gas solute flows up while a liquid solvent flows down the interspaces of a collection of corrugated sheets. A continuous film pattern enhances the interface area between liquid and gas; as a result, the mass transport process is incentivated. On the other hand, increasing the liquid flow rate over a certain threshold may reduce the void area, with a sudden increase of the pressure drop on the gas side (flooding condition). Simplified models usually assume a continuous film covering the solid wall of a flow channel [6, 7], resulting in higher values of the predicted absorption rate. A number of experimental analyses investigates both the break of an initially continuous film covering an inclined plate [8, 9] and the occurrence of finger instability when an advancing film front falling down an inclined plate is perturbed [10]. However, experiments do not allow to access the details of the flow pattern inside the structured packing. On the other hand, the numerical approach is a valuable option to predict the occurrence of film instability in complex geometries such as the one characterizing structured packing, with the eventual break of the continuous wetting layer or the formation of stationary rivulets. A liquid layer falling down an inclined plate bounded by lateral wall, which is the simplest configuration describing the hydrodynamics inside structured packing, was numerically investigated in [3, 5] using a fully 3D CFD analysis, which includes the Volume of Fluid (VoF) method to solve the liquid-gas interface. A large portion of a corrugated sheet was investigated in [4], using the VoF method incorporated in Ansys Fluent®. However, only few configurations were tested due to the large computational cost deriving from the fully 3D modelization. Lubrication theory, which allows to reduce the 3D physical problem of a thin

liquid layer flowing on a hydrophilic surface to a 2D mathematical problem, represents the main tool to predict the instability of a flowing film [11, 12, 13, 14]. The effect of the surface wettability was included in the lubrication framework in [15, 16, 17] through the disjoining pressure [18, 19]. However, such analyses are limited to low values of the contact angle, since the standard small slope approximation does not provide accurate results for $\theta \geq 30°$ [20]. It was proved in [21] that the implementation of the exact free surface curvature allows to investigate contact angles up to 60°, which falls in the range of structured packing applications. A vertical plate bounded by lateral walls, representative of the hydrodynamics inside structured packing, was numerically investigated in [21, 22] via the lubrication theory. Compared to the fully 3D modelization, it was proved in [23, 21] that the lubrication theory allows a great reduction of the computational cost, still providing accurate results for contact angles up to 60°.
Here, a liquid film flowing down a corrugated sheet, which is the basic element of structured packing, is numerically investigated via the lubrication theory. Following [21, 22, 24], the full implementation of the free surface curvature combined with the disjoining pressure model is used to investigate increased surface wettabilities, compared to the range of the standard formulation of the lubrication theory. Compared to previous literature analyses, a non-uniform gravity field is implemented in order to model the corrugated surface, providing a specific tool to study hydrodynamics in structured packing. Thus, the stationary liquid pattern is computed for different geometries and the influence of the corrugated geometry on the eventual dewetting (i.e. formation of stable rivulets) is discussed, since it is a crucial aspect for a proper design of the packing tower, used for absorption and distillation process.

2 Mathematical model

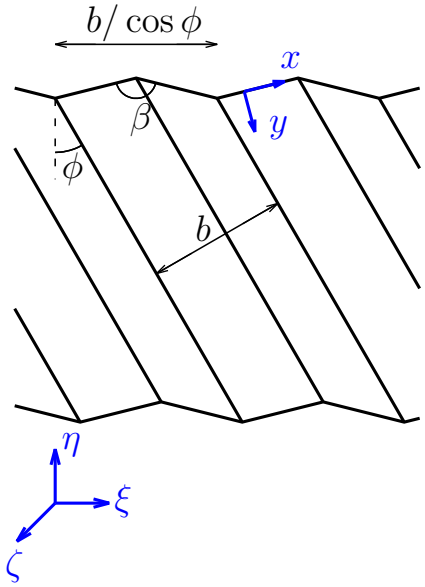

Figure 1: Geometry of a vertical corrugated sheet: crimp angle ϕ, corrugation angle β and corrugation length b. Reference Cartesian coordinate system $O\xi\eta\zeta$ and body-fitted orthogonal coordinate system Oxy laying on the solid surface.

Consider a thin film flowing down a vertical corrugated sheet like the one of Figure 1. Let h be the film thickness and $\mathbf{x} = (x, y)$ be a body-fitted orthogonal coordinate system laying on the corrugated sheet. The lubrication theory allows to integrate the continuity equation across the film thickness. Further assuming a low film Reynolds number gives a parabolic velocity profile across the film thickness, which can be averaged and substituted in the integrated continuity equation yielding the well-known lubrication equation,

$$\frac{\partial h}{\partial t} + \nabla \cdot \left(\frac{\rho\, g\, h^3}{3\,\mu}\, \tilde{\mathbf{g}} - \frac{\nabla p}{3\,\mu}\, h^3 \right) = 0,\ p = -2\,\sigma\ (\kappa + \kappa_s) - D + \rho\, g\, h\ (\hat{\mathbf{g}} \cdot \hat{\mathbf{n}}) \tag{1}$$

where $\tilde{\mathbf{g}}$ is projection of the gravity versor $\hat{\mathbf{g}}$ on the corrugated sheet, $\hat{\mathbf{n}}$ is the normal inward versor, $2\,\kappa_s$

is the solid surface curvature, $2\,\kappa$ is the free surface curvature and D is the disjoining pressure,

$$2\,\kappa = \frac{\frac{\partial^2 h}{\partial x^2}\left[1+\left(\frac{\partial h}{\partial y}\right)^2\right] + \frac{\partial^2 h}{\partial y^2}\left[1+\left(\frac{\partial h}{\partial x}\right)^2\right] - 2\,\frac{\partial h}{\partial x}\,\frac{\partial h}{\partial y}\,\frac{\partial^2 h}{\partial x \partial y}}{\left[1+\left(\frac{\partial h}{\partial x}\right)^2+\left(\frac{\partial h}{\partial y}\right)^2\right]^{3/2}} \tag{2}$$

$$D = B\left[\left(\frac{d}{h}\right)^n - \left(\frac{d}{h}\right)^m\right],\ B = \frac{\sigma}{d}\,\frac{(n-1)\,(m-1)}{n-m}\,(1-\cos\theta) \tag{3}$$

with $n > m > 1$. Compared to the standard formulation of the lubrication theory, the full curvature implementation replaces the small slope approximation, $2\,\kappa = \nabla^2 h$, allowing accurate investigation of contact angles up to 60° [21, 24], while the disjoining pressure models the surface wettability [15, 16]. The presence of a precursor film of thickness $d \ll h$ allows the modelization of moving contact lines. Since the body-fitted orthogonal coordinate system Oxy stands on a corrugated geometry, $\tilde{\mathbf{g}}$ and $\hat{\mathbf{n}}\cdot\hat{\mathbf{g}}$, i.e. the projections of the gravity versor $\hat{\mathbf{g}}$ along the corrugated surface and along its normal inward versor, depend on the position x, y. Introducing the following non-dimensional quantities,

$$\begin{aligned} &H = \frac{h}{h_0},\ \delta = \frac{d}{h_0},\ \mathbf{X} = \frac{\mathbf{x}}{L_0},\ T = \frac{t}{(L_0/u_0)},\\ &P = \frac{p}{\left(\sigma\,h_0/{L_0}^2\right)},\ 2\,K = \frac{2\,\kappa}{\left(h_0/{L_0}^2\right)},\ \Pi = \frac{D}{(\sigma/h_0)} \end{aligned} \tag{4}$$

with h_0 being the undisturbed film thickness, u_0 being the undisturbed film velocity and L_0 being the scaling length,

$$u_0 = \frac{\rho\,g\,{h_0}^2}{3\,\mu},\ L_0 = \left(\frac{\sigma\,h_0}{\rho\,g}\right)^{1/3} \tag{5}$$

the governing lubrication equation can be recast in non-dimensional form,

$$\frac{\partial H}{\partial T} + \nabla\cdot\left(H^3\,\tilde{\mathbf{g}} - H^3\,\nabla P\right) = 0,\ P = -2\,(K+K_s) - (3\,\mathrm{Ca})^{-2/3}\,\Pi + (3\,\mathrm{Ca})^{1/3}\,H\,(\hat{\mathbf{g}}\cdot\hat{\mathbf{n}}) \tag{6}$$

with Ca being the film capillary number, $\mathrm{Ca} = \mu\,u_0/\sigma$.
An in-house code, previously developed in `FORTRAN` and validated with experimental evidence [23, 21, 24], is used to numerically solve Eq. (6) on an orthogonal, structured grid via finite volume method (FVM). A second order centered scheme such as the one of [25] was implemented for spatial discretization, while the Alternate Direction Implicit (ADI) approximate factorization of [26] was used for marching in time. Parallelization for a shared memory machine was achieved via the OpenMP interface.

3 Numerical setup

Figure 1 shows the reference geometry of a corrugated sheet, defined by: the crimp angle ϕ between the corrugation direction and the vertical one; the surface corrugation angle β; the corrugation length b, i.e. the distance between two consecutive peaks or valleys. The governing lubrication equation is solved on the body-fitted orthogonal coordinate system Oxy laying on the corrugated surface, with x denoting the horizontal direction. The projection of the gravity versor $\hat{\mathbf{g}}$ along the corrugated sheet surface is required in order to implement the hydrostatic pressure in Eq. (6),

$$\tilde{\mathbf{g}} = \begin{Bmatrix}\hat{\mathbf{g}}\cdot\hat{\mathbf{i}}\\ \hat{\mathbf{g}}\cdot\hat{\mathbf{j}}\end{Bmatrix},\ \hat{\mathbf{g}}\cdot\hat{\mathbf{i}} = 0,\ \hat{\mathbf{g}}\cdot\hat{\mathbf{j}} = \sqrt{1-(\hat{\mathbf{n}}\cdot\hat{\mathbf{g}})^2} \tag{7}$$

with $\hat{\mathbf{n}}$ being the normal inward versor to the corrugated sheet surface and $\hat{\mathbf{i}}$, $\hat{\mathbf{j}}$ being versors directed along x, y axes. Since the straightforward calculation of the substrate curvature, $2\,\kappa_s = -\nabla\cdot\hat{\mathbf{n}}$, would lead to a numerical discontinuity in correspondence of the sharp corrugations, a dummy smoothing radius of $r = b/15$, is used only for the implementation of the substrate curvature, required by the governing lubrication equation. The computational domain is composed of a portion of the corrugated sheet of non-dimensional size $L_X \times L_Y$. The liquid is injected through the topmost section, located at $Y = 0$, through which the undisturbed film thickness and film flux are imposed: $H = 1$, $\mathbf{Q}\cdot\hat{\mathbf{n}} = 1$, with $\hat{\mathbf{n}}$

denoting the normal to the inlet section and $\mathbf{Q} = H^3\ (\tilde{\mathbf{g}} - \nabla P)$ being the non-dimensional film flux. A fully developed flow is imposed through the bottomest section, $Y = L_Y$, where $\nabla H \cdot \hat{\mathbf{n}} = 0$, $\nabla P \cdot \hat{\mathbf{n}} = 0$. Periodic boundary conditions are implemented through sections $X = 0$, L_X. Since the corrugated sheet geometry is recursive, L_X must be a multiple of the periodic length for a proper implementation of the periodic boundary conditions:

$$X_\pi = \sqrt{\left(\frac{b/L_0}{\cos\phi}\right)^2 + \left(\frac{b/L_0}{\tan\left(\beta/2\right)}\right)^2} \tag{8}$$

A dry domain is always initialized at $T = 0$. This means that the solid substrate is initially covered by the precursor film: $H(X,Y)|_{T=0} = \delta$. Following literature, the disjoining exponents are set to $n = 3$, $m = 2$, while the non-dimensional precursor film thickness is set to $\delta = 5 \times 10^{-2}$. After a grid independence analysis, it was verified that a spatial discretization step of ΔX, $\Delta Y \leq \delta$ is required to get accurate results. The computational domain dimensions are set to $L_X = 2\,X_\pi$ and $L_Y = 50$, with X_π being the periodic length of the corrugated geometry, evaluated along x direction via Eq. (8). The condition $L_X > \lambda_{cr}$ is verified for all the investigated geometries, with $\lambda_{cr} \simeq 7.86$ being the critical wavelength of the spanwise perturbations [16]: this allows to observe the finger instability phenomenon and, thus, to accurately predict the eventual dewetting of the domain, which defines the transition between continuous film and rivulet regime.

4 Result

Parametric computations are run at different corrugated sheet geometries and flow conditions, the latter being defined by the Capillary number and by the static contact angle. The stationary flow pattern is traced, in order to analyse possible transitions from a continuous film to an ensemble of rivulets. In particular, three corrugation angles are investigated, $\beta = 90°$, $113°$ and $143°$, while the non-dimensional corrugation length and the crimp angle are set to $b/L_0 = 12$ and $\phi = 45°$. The film capillary number is ranged in $10^{-2} \div 5 \times 10^{-2}$, while the static contact angle is set to $\theta = 45°$. The imposed parameters are consistent with real test cases involving CO2 absorption through structured packing: as an example, Ca of the order of 5×10^{-2} covers the typical application described in [5], while b/L_0 in the range [12, 20] were addressed in [4].

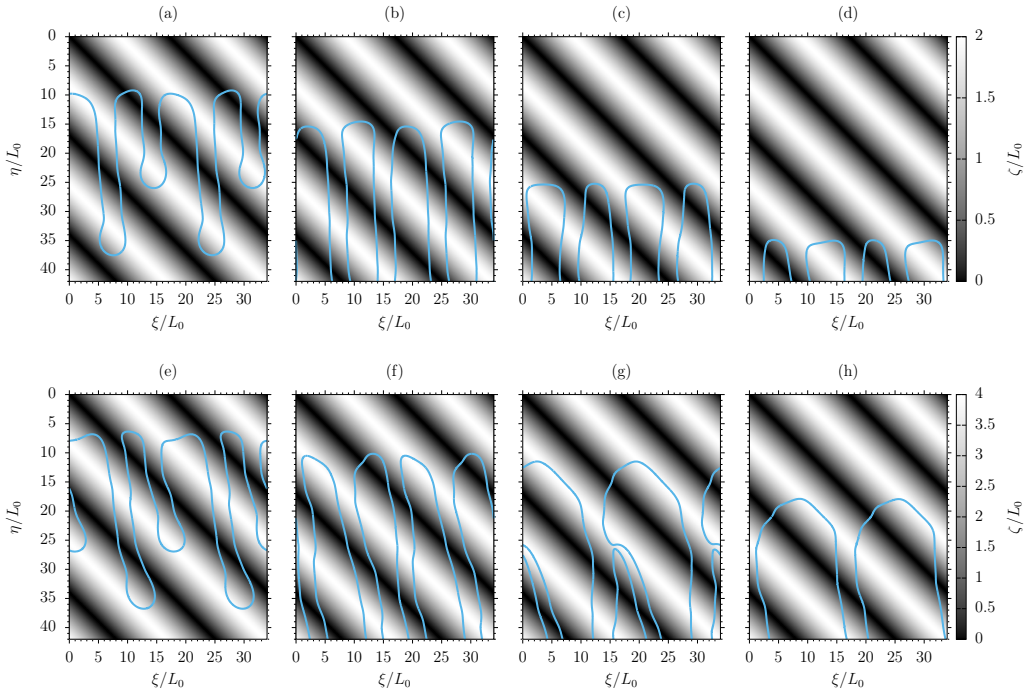

Figure 2: Contact line evolution at successive instants: $\beta = 143°$ (a-d); $\beta = 113°$ (e-h). $T = 20$, 40, 80, 120. $\theta = 45°$, $\mathrm{Ca} = 3 \times 10^{-2}$, $b/L_0 = 12$, $\phi = 45°$.

Figure 2 compares the moving contact line at successive instants, for the same $\mathrm{Ca} = 3 \times 10^{-2}$, $b/L_0 = 12$ and different corrugation angles: $\beta = 143°$, which corresponds to a corrugation height of $b/6$, and $\beta = 113°$, which corresponds to $b/3$. The stationary solution of both the configurations is characterized by a continuous film wetting the whole domain. As could be expected, the rivulets drain faster at lower corrugation height, meaning that the vertex between two neighbor rivulets moves downward with a higher velocity. Furthermore, the rivulets move essentially along the η direction when $\beta = 143°$, while they start to deviate, following the corrugation direction for $\beta = 113°$. This is due to the combined effect of gravity and surface tension. Indeed, the local substrate curvature induces additional capillary forces, that drive the liquid into the valleys of the corrugated sheet. A change in the number of rivulets is also reported: 4 rivulets are observed at high β, that is consistent with the one predicted via a stability analysis of a falling film subjected to spanwise perturbation such as the one of [16], $L_X/\lambda_{cr} = 4.4$ with $\lambda_{cr} \simeq 7.86$; 2 rivulets are observed at low β, meaning that film stability is influenced by the presence of the corrugations.

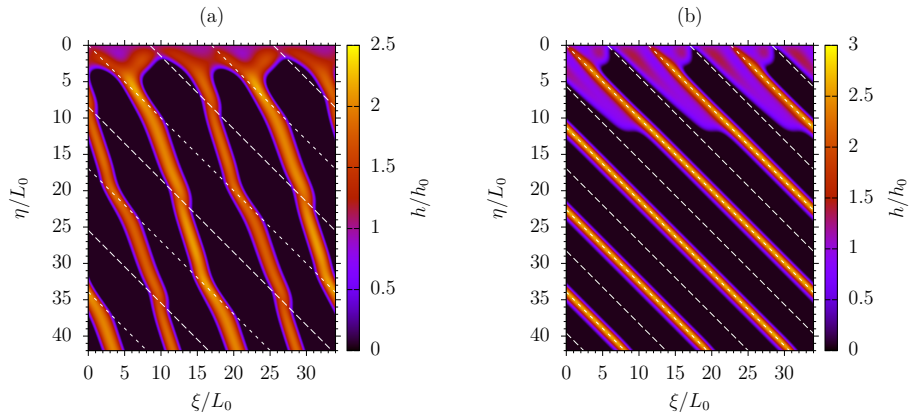

Figure 3: Stationary liquid layer distribution: $b/L_0 = 12$, $\theta = 45°$ (a); $b/L_0 = 8$, $\theta = 30°$ (b). $\mathrm{Ca} = 3 \times 10^{-}$, $\beta = 90°$, $\phi = 45°$. Dashed lines denotes valleys (short hatch) and peaks (long hatch) of the corrugated surface.

Indeed, when $\beta = 90°$, i.e. corrugation height equal to $b/2$, we observe a partial dewetting of the computational domain (i.e. receding front forms between two neighbor rivulets), covered by 4 stationary rivulets. The steady state solution for $\mathrm{Ca} = 3 \times 10^{-2}$, $b/L_0 = 12$ and $\beta = 90°$ is shown in Figure 3(a). The effect of the film Capillary number is shown in Figure 4, which refers to $\mathrm{Ca} = 4 \times 10^{-2}$, while the non-dimensional geometry is the same as Figure 3(a), i.e. $b/L_0 = 12$, $\beta = 90°$ and $\phi = 45°$: slightly increasing Ca, a change in the liquid flow pattern is observed, with the 4 rivulets, formed due to the perturbance induced by the corrugations, merging into to 2 rivulets, that slowly drain down the vertical corrugated sheet.

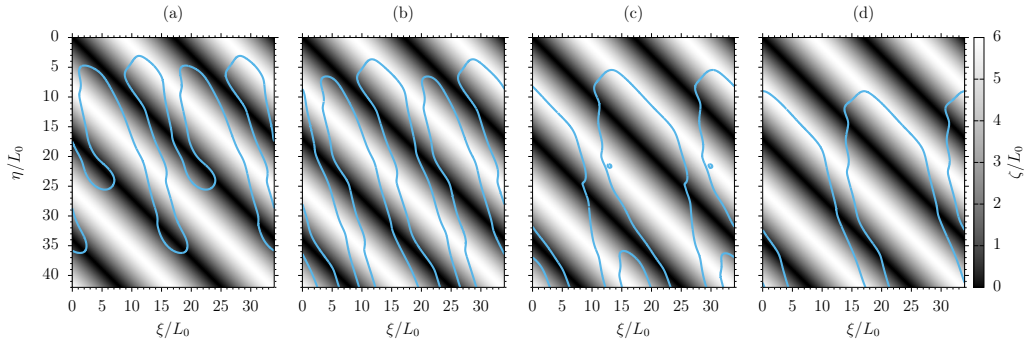

Figure 4: Contact line evolution at successive instants: $T = 20$ (a), $T = 40$ (b), $T = 80$ (c), $T = 120$ (d). $\theta = 45°$, $\mathrm{Ca} = 4 \times 10^{-2}$, $b/L_0 = 12$, $\beta = 90°$, $\phi = 45°$.

The flow pattern is traced as a function of both the Capillary number Ca and the corrugation angle β

in Table 1, which proves that the corrugation geometry affects the observed flow pattern: a continuous film, incentivated by choosing lower β, enhance the mass transfer process during the absorption process; however, lowering β decreases the corrugated sheet surface (i.e. the potential liquid-gas interface area) and may induce flooding occurrence, with an increase of the pressure drop and the possible obstruction of the gas flow. For Ca $= 0.04$, $\beta = 90°$, the vertices between two neighbor rivulets, formed due to finger instability, move downward with a small velocity $u/u_0 < 0.1$, see Figure 4, meaning that we are very close to the transition from film to rivulet regime

Ca \ β	90°	113°	143°
0.02	*	*	*
0.03	*	⋆	⋆
0.04	⋆	⋆	⋆
0.05	⋆	⋆	⋆

Table 1: Flow pattern map: the red asterisks denote a rivulet pattern; the blue stars denote a continuous film pattern. $\theta = 45°$, $b/L_0 = 12$, $\phi = 45°$.

An additional computation is run, in order to investigate the effect of changing the corrugation length b. Figure 3(b), referred to $b/L_0 = 8$ and $\theta = 30°$, shows a different behavior, if compared to the test case of Figure 3(a), even though a partial dewetting of the computational domain is observed in both the two cases. Indeed, the stationary rivulets follow the corrugation direction for the lower value of b, while a small deviation from the vertical direction is observed for the stationary rivulets at $b/L_0 = 12$ and the same Ca and β, see Figure 3(a). The wetted area fraction of the stationary liquid distribution is also computed for both $b/L_0 = 12$ and $b/L_0 = 8$, given that decreasing the corrugation length lowers the wetted area of about 12% and, thus, worsens the mass transfer. On the other hand, such a configuration diminishes the risk of flooding, since interference or coalescence between the rivulets flowing down adjacent, corrugated sheets is avoided.

5 Conclusion

The evolution of a liquid layer down a corrugated sheet, which is the characteristic configuration of structured packing, was investigated via the lubrication theory. The reduction to a 2D mathematical model allowed a sensible reduction of the computational cost respecting a fully 3D numerical approach. Compared to previous works, the simulation of a corrugated sheet was possible via the additional implementation of: a non-uniform gravity field in the lubrication framework; an additional force induced by the substrate curvature. The full curvature formulation, together with the disjoining pressure model, allowed to investigate surface wettabilities in the range of applications characterizing absorption through structured packing. Results show that the corrugation geometry affects the liquid flow pattern, which prediction is crucial to estimate the effective mass transfer rate in absorption applications. In particular, it was observed that low corrugation angles incentivate the formation of a continuous wetting layer, but augment the risk of flooding, that dramatically reduces the mass transfer performances. Furthermore, different possible patterns were observed for the rivulet regime, with the liquid moving downward along the vertical direction or following the corrugations, that further decreases the wetted area but avoids the occurrence of flooding.

The proposed modelization represents a novel approach and an effective tool for the design of the structured packing, since real configurations can be accurately investigated with low computational costs. The non-dimensional approach allows to extend results from a single simulation to a family of physical problems (for example, the capillary number is correlated to the liquid flux, given the liquid solvents properties). Parametric computations at different corrugation geometries and flow conditions provide useful statistical information, such as the interface area between solvent and solute, to be used for mapping the optimal geometry as a function of the required mass transfer rate. As a future work, the effect of the shear stress applied by the gas solute, which flows countercurrent to the liquid solvent, should be included, coupling the film solver with the CFD analysis of the core flow. Furthermore, this would allow to accurately predict flooding occurrence, which is as important as the liquid flow pattern over the corrugated sheet.

References

[1] Croce G, De Candido E, Habashi W G, Munzar J, Aubé M S, Baruzzi G S and Aliaga C 2010 *J. Aircraft* **47** 1283–1289
[2] Suzzi N and Croce G 2024 *J. Phys. Conf. Ser.* **2685** 012019
[3] Hoffmann A, Ausner I, Repke J U and Wozny G 2005 *Comput. Chem. Eng.* **29** 1433–1437
[4] Subramanian K and Wozny G 2012 *Int. J. Chem. Eng.* **2012** 838965
[5] Singh R K, Galvin J E and Sun X 2016 *Chem. Eng. Sci.* **142** 244–257
[6] Rocha J A, Bravo J L and Fair J R 1993 *Ind. Eng. Chem. Res.* **32** 641–651
[7] Rocha J A, Bravo J L and Fair J R 1996 *Ind. Eng. Chem. Res.* **35** 1660–1667
[8] Podgorski T, Flesselles J M and Limat L 1999 *Phys. Fluids* **11** 845
[9] Limat L R 2006 *Phys. Fluids* **18** 032102
[10] Johnson M F G, Schluter R A, Miksis M J and Bankoff S G 1999 *J. Fluid Mech.* **394** 339–354
[11] Oron A, Devis S H and Bankoff S G 1997 *Rev. Mod. Phys.* **69** 931–980
[12] Kataoka D E and Troian S M 1997 *J. Colloid Interf. Sci.* **192** 350–362
[13] Beltrame P, Knobloch E, Hänggi P and Thiele U 2011 *Phys. Rev. E* **83** 016305
[14] Ma C and Liu J 2021 *Phys. Fluids* **33** 022101
[15] Schwartz L W and Eley R R 1998 *J. Colloid Interf. Sci.* **202** 173–188
[16] Zhao Y and Marshall J S 2006 *J. Fluid Mech.* **559** 355–378
[17] Sellier M 2015 *Int. J. Multiphas. Flow* **71** 66–73
[18] Blake T D 2006 *J. Colloid Interf. Sci.* **299** 1–13
[19] Bonn D, Eggers J, Indekeu J, Meunier J and Rolley E 2009 *Rev. Mod. Phys.* **81** 739–805
[20] Perazzo C A and Gratton J 2004 *J. Fluid Mech.* **507** 367–379
[21] Suzzi N and Croce G 2019 *Phys. Fluids* **31** 122106
[22] Suzzi N and Croce G 2021 *J. Phys. Conf. Ser.* **1868** 012010
[23] Suzzi N and Croce G 2017 *J. Phys. Conf. Ser.* **923** 012020
[24] Suzzi N and Croce G 2021 *Fluids* **6** 405
[25] Diez J A and Kondic L 2002 *J. Comput. Phys.* **183** 274–306
[26] Witelski T P and Bowen M 2003 *Appl. Numer. Math.* **45** 331–351

Acknowledgments

We wish to acknowledge NextGenerationEU for supporting the present work, performed within the project Interconnected Nord-Est Innovation Ecosystem (iNEST), placed within the context of National Recovery and Resilience Plan (PNRR).